Journal of Environmental Management 286 (2021) 112130

Contents lists available at ScienceDirect

Journal of Environmental Management

journal homepage: http://www.elsevier.com/locate/jenvman

Photocatalytic hydrogen production by ternary heterojunction composites of silver nanoparticles doped FCNT-TiO_2

N.Ramesh Reddy [a], U. Bharagav [b], M.V. Shankar [b], P. Mohan Reddy [a], Kakarla Raghava Reddy [c], Nagaraj P. Shetti [d], Fernando Alonso-Marroquin [e], M. Mamatha Kumari [b,**], Tejraj M. Aminabhavi [f,*], Sang Woo Joo [a,***]

[a] School of Mechanical and IT Engineering, Yeungnam University, Gyeongsan 38541, Republic of Korea
[b] Nanocatalysis and Solar Fuels Research Lab, Department of Materials Science &Nanotechnology, Yogi Vemana University, Kadapa, 516 005, Andhra Pradesh, India
[c] School of Chemical and Biomolecular Engineering, The University of Sydney, Sydney, NSW 2006, Australia
[d] Center for Electrochemical Science & Materials, Department of Chemistry, K.L.E. Institute of Technology, Hubballi, 580 030, Karnataka, India
[e] School of Civil Engineering, The University of Sydney, NSW 2006, Australia
[f] Soniya College of Pharmacy, Dharwad, Karnataka, 580 002, India

ARTICLE INFO

Keywords:
TiO_2 nanoparticles
Silver nanoparticles
CNTs
Chemical reduction
Photocatalysis
Hydrogen production

ABSTRACT

Silver nanoparticles doped with FCNT-TiO_2 heterogeneous catalyst was prepared via one-step chemical reduction process and their efficacy was tested for hydrogen production under solar simulator. Crystallinity, purity, optical properties, and morphologies of the catalysts were examined by X-Ray diffraction, Raman spectroscopy, UV–Visible diffuse reflectance spectra, and Transmission Electron Microscopy. The chemical states and interface interactions were studied by X-ray photoelectron spectroscopy and Fourier transform infrared spectroscopy. The optimized catalyst showed 19.2 mmol g^{-1} h^{-1} of hydrogen production, which is 28.5 and 7 times higher than the pristine TiO_2 nanoparticles and FCNT-TiO_2 nanocomposite, respectively. The optimized catalyst showed stability up to 50 h under the solar simulator irradiation. The natural solar light irradiated catalyst showed ~2.2 times higher hydrogen production rate than the solar simulator irradiation. A plausible reaction mechanism of Ag NPs/FCNT-TiO_2 photocatalyst was elucidated by investigating the beneficial co-catalytic role of Ag NPs and FCNTs for enhanced hydrogen production.

1. Introduction

In efforts to protect the environment from the adverse impacts of fossil fuels, researchers have been developing new energy sources, such as supercapacitors, batteries, and hydrogen (H_2) fuel (Rudzinski and Aminabhavi, 2000). In these efforts, H_2 fuel is one of exciting energy source because of its cost-effectiveness, eco-friendly nature, and stress-free production (Mehta et al., 2019; Xue et al., 2020). Moreover, H_2 contributes to the creation of benign environment due to its zero-emission, and also reduces the dependence on non-renewable resources. In recent years, photocatalysis has been widely studied for H_2 production due to its environmental friendly process and simplistic approach Bellamkonda et al. (2019); Mishra et al. (2019); Rao et al. (2019), (Cavalcanti et al., 2019).

TiO_2 semiconductor has all the required properties for photocatalysis due to its versatile thermal, physical, and chemical properties in addition to being inexpensive, eco-friendly, abundantly available and long-term stability (Lakshmana Reddy et al., 2016; Mandari et al., 2018). There is thus an urgent need to improve H_2 production via photocatalysis because the adverse effects of photocatalysts, such as large energy band gaps, fast charge carrier recombination, and narrow light absorption, are limiting factors for achieving scalable H_2 production. The tuning of TiO_2 by the addition of suitable metals, non-metals, noble metals, and other semiconductor materials has been widely explored for its potential applications (Naldoni et al., 2013; Zhao et al., 2014).

The coupling of carbon nanotubes (CNTs) with TiO_2 as a

* Corresponding author.
** Corresponding author..
*** Corresponding author.
E-mail addresses: reddy.chem@gmail.com (K.R. Reddy), mamatha@yogivemanauniversity.ac.in (M.M. Kumari), aminabhavit@gmail.com (T.M. Aminabhavi), swjoo@yu.ac.kr (S.W. Joo).

https://doi.org/10.1016/j.jenvman.2021.112130
Received 13 December 2020; Received in revised form 1 February 2021; Accepted 3 February 2021
Available online 5 March 2021

heterojunction is one of the highly efficient and ongoing strategies for the production of H_2 (Mamathakumari et al., 2015; Ramesh Reddy et al., 2018) because CNTs have unique chemical, thermal, electrical, and optical properties along with high surface area (Liu et al., 2011; Zhang et al., 2013). CNTs reduce the rate of electron-hole recombination by acting as electron sinks. Furthermore, CNTs act as co-catalyst as well as electron transport channels in the photocatalyst (Leary and Westwood, 2011). Zhao et al. reported remarkable H_2 production using Pt-carbon/TiO_2 nanotube/carbon nanotubes photocatalyst (Zhao et al., 2014), wherein CNTs and Pt acted as co-catalysts and electron sinks, thereby improving the H_2 production efficiency.

From literature, it is evident that preparation of ternary nanocomposites represents a powerful strategy to enhance H_2 production efficiency (Mokhtar Mohamed et al., 2015; Sangari et al., 2015). Noble metal Pt is a very effective co-catalyst that was used to enhance H_2 production, but Pt is highly expensive and is not abundantly available. However, for large-scale applications, it is necessary to replace Pt with the low-cost and highly available materials. Hence, silver (Ag), which also belongs to the noble metal family, being less expensive and abundant material than Pt, Ag could be used to replace Pt as co-catalyst. However, nanostructures of Ag have attracted enormous attention in health care, energy, robotic and environmental areas (Augustine and Hasan, 2020; Marimuthu et al., 2020; Suh et al., 2019).

Surface plasmon resonance (SPR) effect is advantageous to enhance the H_2 production efficiency. The plasmonic photocatalysts have the heterogeneous/Schottky junction as well as localized surface plasmon resonance (LSPR) (Hao et al., 2018), and the resulting junctions can effectively reduce the recombination of photogenerated charge carriers by producing an internal electric field. Further, LSPR junction extend the TiO_2 absorption region towards the visible region (Kumar et al., 2016a; Sreekanth et al., 2016). Chaudhary et al., reported Ag/CNT-TiO_2 ternary nanocomposites for methylene blue dye degradation under UV and visible light irradiation (Chaudhary et al., 2016a). Abdulrajak et al., reported the Pt-CNT/TiO_2 photocatalyst for H_2 production, which was prepared by sonochemical/hydration-dehydration process (Abdulrazzak et al., 2016).

In this research, visible active and highly stable Ag nanoparticles (AgNPs) doped FCNT-TiO_2 ternary photocatalyst were prepared via one-pot chemical reduction method. Earlier, such ternary nanocomposites were synthesized by either two or three-step chemical methods (Ishaq et al., 2019; Yang et al., 2014), which required longer time and had different chemical reaction pathways, thereby realizing that ternary photocatalyst synthesis is an attractive strategy through one-pot synthesis. In view of these considerations, a one-pot chemical reduction method calcined under open air and inert atmosphere was used here for the preparation of AgNPs/FCNT-TiO_2 ternary photocatalyst for photocatalytic H_2 production.

2. Experimental procedure

2.1. Materials and reagents

Analytical grade chemicals were utilized without any further purification for the catalyst synthesis, while functionalized Multiwalled Carbon nanotubes (FCNTs) were purchased from Global Nanotech. Titanium butoxide (TBOT) was used as titanium source, purchased from Sigma Aldrich. Silver nitrate ($AgNO_3$) was used as a silver precursor and was purchased from Merck India. Ethanol and sodium borohydride ($NaBH_4$) were purchased from Merck, India. Distilled water (DW) and battery water (LIMARA Kadapa, India) were utilized for all the materials synthesis as well as hydrogen generation experiments. The hole scavenger glycerol was purchased from Merck, India.

2.2. Synthesis of AgNPs doped FCNT-TiO_2 heterojunction composite

The Ag-doped FCNT-TiO_2 photocatalysts were synthesized by a one-step chemical reduction method in which FCNTs and TBOT were dispersed in DW and ethanol, individually by sonication and stirring. After thorough dispersion TBOT was then added dropwise to the dispersed FCNTs solution. Next, freshly prepared 0.5 M of $NaBH_4$ solution was added dropwise to the above mixture. Then, 1 mL $AgNO_3$ solution taken out from 200 mM $AgNO_3$ aqueous solution and was added dropwise to the above mixture under stirring, which was continued for further 2 h. The total solution was transferred into an RB flask, which was kept in the oil bath and the total solution was heated at 60 °C (±4 °C) for 5 h on a hot plate magnetic stirrer. After completing the reaction, the resultant mixture was washed with HCl, DW, and ethanol. Obtained final product was dried at 80 °C for 10 h. The dried product was calcined at 450 °C for 2 h under N_2 and open-air atmospheres. By varying the concentration of silver, Ag/FCNT-TiO_2 composite catalysts were prepared and synthesis schematic is shown in Fig. 1. The compositions and abbreviations of all the synthesized catalysts are given in Table 1.

2.3. Characterization

The supplementary information provides a detailed description of the characterization techniques used.

2.4. Photocatalytic hydrogen experiments

All the photocatalytic H_2 production experiments were carried out in a 185 ml quartz reactor under Solar simulator and natural sunlight irradiation (Praveen Kumar et al., 2015; Rao et al., 2018). 5 mg of the catalyst was dispersed in 5 vol% glycerol aqueous solution by stirring and then the quartz reactor was latched with a gas-tight rubber septum. The reactor was outgassed with a vacuum pump and purged with high purity N_2 gas. The quartz reactor was kept in a solar simulator (300 W Xenon lamp) for upto 4 h. The resultant H_2 gas in the reactor was collected at 1h time interval with a 250-μl syringe and then analyzed with the offline gas chromatography (Shimadzu GC-2014), equipped with a thermal conductivity detector (TCD) and a molecular sieve/5Å column, at 70 °C and using N_2 carrier gas.

3. Results and discussions

3.1. Crystallinity analysis

The crystallinity of the catalysts was evaluated by XRD, The XRD patterns for AT, FT, AFT-N_2, and AFT-OA catalysts are shown in Fig. 2a. The 2θ values of TiO_2 appear at 25.3, 37.8, 48.1, 54.9, 62.9, 67.4, and 75.1°, which are assigned to A(101), A(004), A(200), A(211), A(204), A (116), and A(251) planes respectively. The 2θ values and the related XRD planes correspond to the standard anatase JCPDS card No. 21–1272 and reported in the literature (Aphairaj et al., 2011; Bi and Liu, 2019). The TiO_2 anatase planes also appear in AT, AFT-OA, and AFT-N_2 catalysts along with the new peaks at 27.7, 32.1, 45.8, and 56.9°, which are ascribed to Ag(210), Ag(113), Ag(124), and Ag(240) planes, respectively (Karthik et al., 2014), suggesting the successful inclusion of Ag NPs in FCNT-TiO_2 nanocomposite. The absence of carbon peak in XRD may be due to its low concentration in the composition and/or lower XRD intensity compared to TiO_2 and Ag NPs. The carbon presence in the catalyst was further confirmed by TEM and XPS results.

Fig. 2b represents Raman spectra of TiO_2, AT, AFT-N_2, and AFT-OA catalysts. Raman peaks of TiO_2 showing at ~138, 196, 386, 506, and 629 cm^{-1} are associated with TiO_2 anatase modes of $E_{g(1)}$, $E_{g(2)}$, $B_{1g(1)}$, A_{1g} + $B_{1g(2)}$, and $E_{g(3)}$, respectively. The obtained anatase modes are well-matched with the XRD data and also with the previous reports reported elsewhere (Lubas et al., 2014; Tuschel, 2019). In case of AT, AFT-N_2, and AFT-OA composites, the Raman intensity was reduced compared to TiO_2. The reduced Raman intensities are due to the halting of lattice periodicity and translational crystal symmetry that has

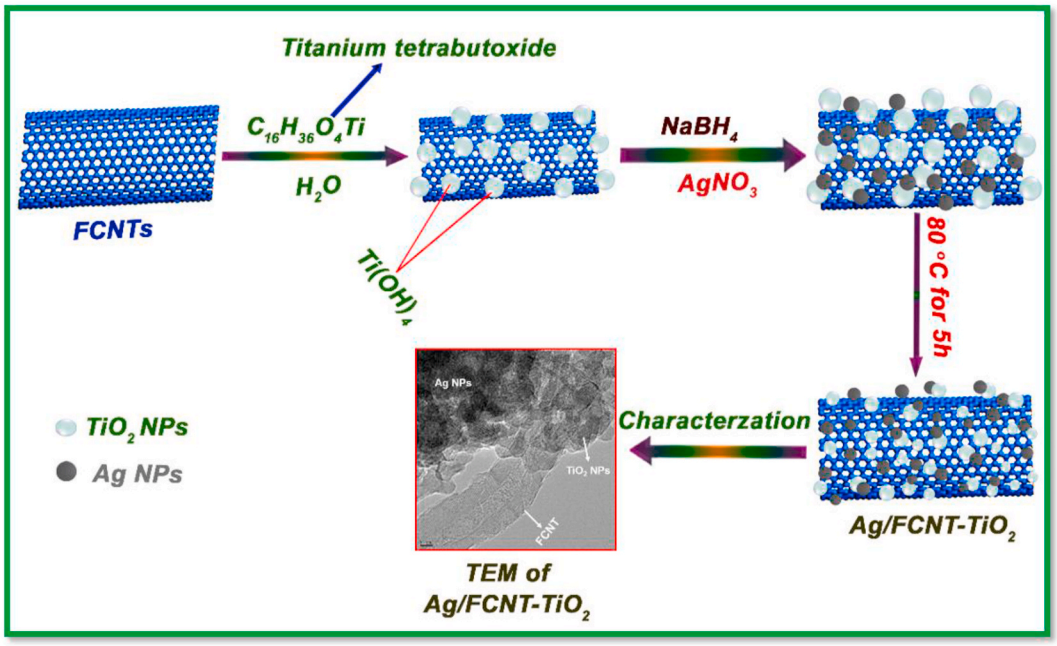

Fig. 1. Schematic representation of the synthesis procedure for Ag/FCNT-TiO_2 heterogeneous photocatalyst.

Table 1
Nominal compositions and abbreviations for the photocatalyst tested in the present study.

Photocatalyst	Nomenclature
Synthesized TiO_2 nanoparticles	TiO_2
FCNT-TiO_2	FT
Silver (Ag)– TiO_2	AT
1 ml silver added FCNT-TiO_2-Dried	AFT-D
1 ml silver added FCNT-TiO_2 calcined under muffle furnace (open-air)	AFT-OA
1 ml silver added FCNT-TiO_2 calcined under N_2 atmosphere	AFT-N_2/AFT-3
0.5 ml Silver added FCNT-TiO_2	AFT- 1
0.75 ml Silver added FCNT-TiO_2	AFT- 2
1 ml Silver added FCNT-TiO_2	AFT- 3
1.25 ml Silver added FCNT-TiO_2	AFT- 4
1.5 ml Silver added FCNT-TiO_2	AFT-5

produced defects in the crystal lattice due to the addition of FCNTs and AgNPs (Chaudhary et al., 2016a). Su et al., also reported the Raman spectra with lower intensity for Ag/TiO_2, compared to that of pristine TiO_2 due to the addition of Ag to the crystal lattice. (Su et al., 2012). Moreover, the inset of Fig. 2b presents the Raman spectra of AFT-OA and AFT-N_2 . These results confirm the presence of TiO_2 anatase peaks 196, 386, 506 and 629 cm^{-1} in AFT-OA and AFT-N_2 catalysts (Fig. 2b). Moreover, AFT-N_2 showed lower intensity than AFT-OA, indicating strong interaction of FCNTs with TiO_2 than in AFT-OA catalyst (Chaudhary et al., 2016b; Liu et al., 2016). This is because under N_2 atmosphere, carbon may not decompose and produce a strong interface with AgNPs and TiO_2.

3.2. Morphology analysis

In order to investigate the morphological properties as well as the distribution of Ag and TiO_2 nanoparticles on FCNT in AFT-N_2 catalyst, TEM characterization was performed (Fig. 3) TEM images revealed the deposition of Ag and TiO_2 nanoparticles onto the surface of FCNTs (see Fig. 3a, b and c). The spotted lines (A1, A2, A3, and A4) from the high-resolution spectra (Fig. 3d) and d-spacing values were calculated from the inverse fast fourier transformation (IFFT) using the digital micrograph software. The IFFT images of A1, A2, A3, and A4 spotted lines and

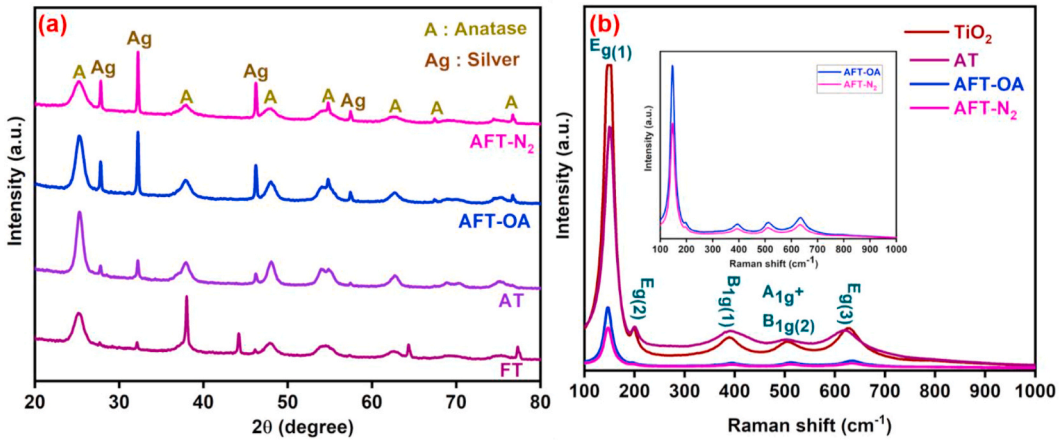

Fig. 2. (a) XRD pattern of FT, AT, AFT-N_2, and AFT-OA catalysts and (b) Raman spectra of TiO_2, AT, AFT-N_2, and AFT-OA catalysts (inset is AFT-N_2 and AFT-OA).

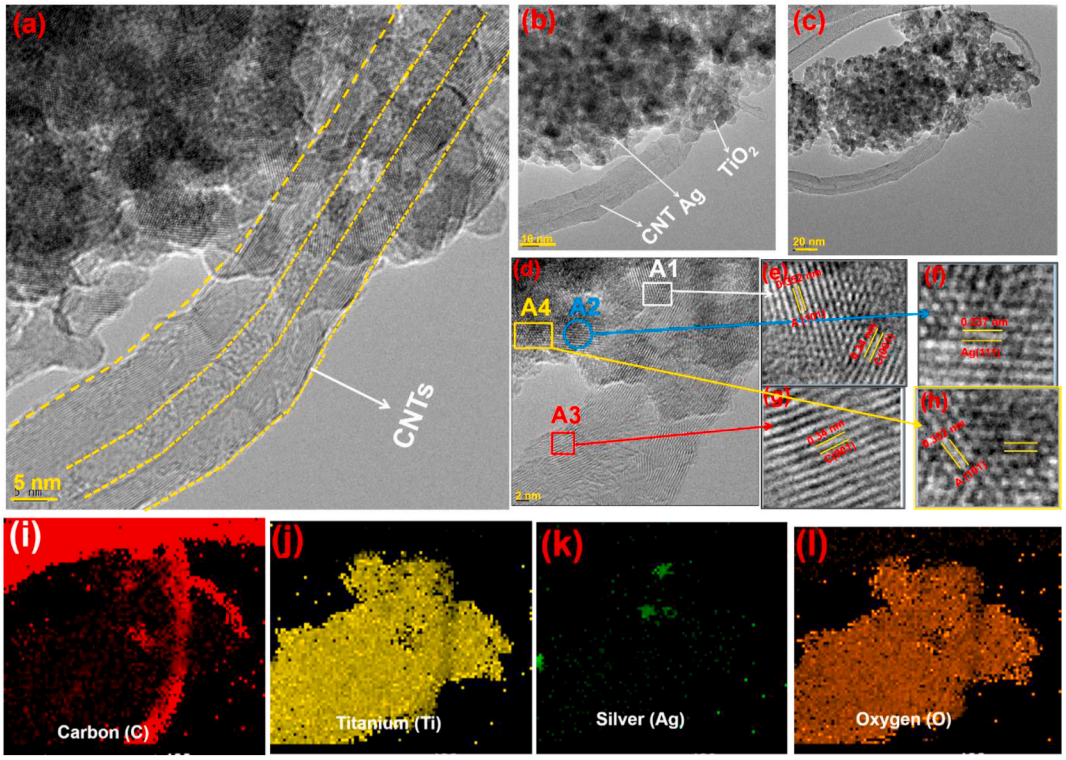

Fig. 3. TEM images of AFT-N_2 (a–d) at different magnifications, (e–h) selected areas IFFT, respective d-spacing values, and elemental mapping of (i) C, (j) Ti, (k) Ag, and (l) O elements.

those corresponding d-spacing values are shown in Fig. 3e, f, 3g, and 3h, respectively. From these, the resultant d-spacing values were 0.352, 0.34, and 0.23 nm corresponding to A(101), C(001), and Ag(111) planes, respectively. Interestingly, the mixed crystalline planes were observed from Fig. 3e and h, indicating strong interface interaction between AgNPs, TiO_2, and CNT. Further, elemental distribution in the catalysts was examined by elemental mapping analysis and correspondingimages were shown in Fig. 3i-l which revealed the equal distribution of the elements in the composite, thus confirming the presence of Ag, Ti, O and carbon in AFT.

3.3. Optical properties

Optical properties such as absorption region and band gaps were analyzed for TiO_2, FT, AT, AFT-OA, and AFT-N_2 by UV–visible Diffuse Reflectance Spectroscopy (DRS). As can be seen in Fig. 4a, TiO_2 absorption wavelength augmentation was observed after the addition of both FCNT and Ag nanoparticles. AFT-N_2 catalysts showed extended absorption range compared to other photocatalysts, and this might be due to the calcination of the composite under inert atmospheric conditions, thus making a strong interface interaction of FCNTs with the nanoparticles of Ag and TiO_2. The open-air calcined AFT-OA ternary catalyst showed slightly lower absorbance than the AFT-N_2, due to the decomposition of FCNTs in open-air atmospheric conditions, which agreed well with the literature findings (Li et al., 2014; Tranchard et al., 2017) as well as the XPS results (based on the resultant carbon atomic weight % in the catalyst).

The energy band gaps were calculated for the synthesized catalysts

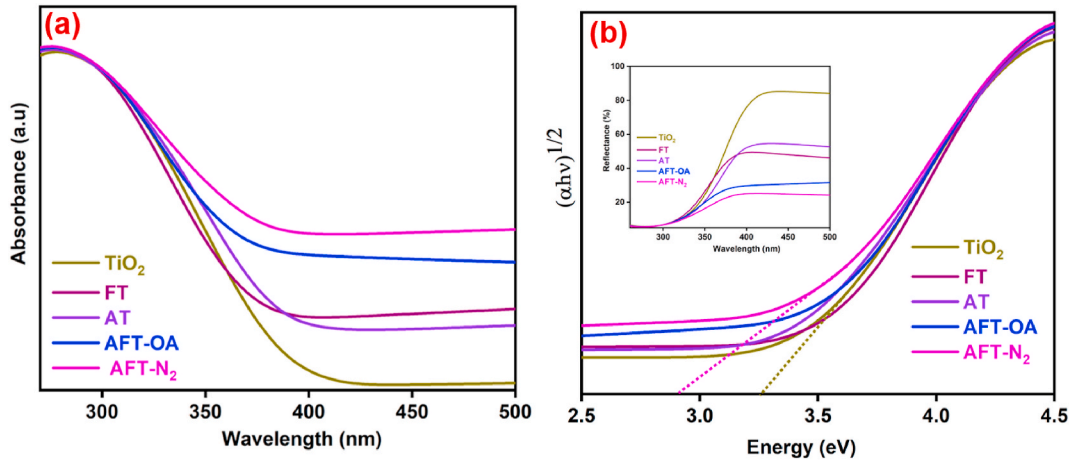

Fig. 4. UV-Visible DRS (a) absorption spectra of TiO_2, FT, AT, AFT-OA, and AFT-N_2 catalysts, (b) calculated energy band gap values of TiO_2, FT, AT, AFT-OA, and AFT-N_2 catalyst through kubelka munk relation, reflectance spectra of TiO_2, FT, AT, AFT-OA and AFT-N_2 catalysts in the inset.

using the resultant plots of Kubelka-Munk function derived from UV–visible DRS as shown in Fig. 4b. The band gap values of the composite was reduced compared to pristine TiO_2. The reduced bandgap value of the optimized catalyst is 2.9 eV (AFT-N_2). However, the FT catalyst showed a slightly higher energy bandgap than the pristine TiO_2 due to the screeing effect of the other nanoparticles limiting the effective absorbance of light and poor interaction of FCNTs with TiO_2. . On the other hand, due to the surface plasmon resonance (SPR) effect of AgNPs, the AT catalyst also showed lower band gap than TiO_2. The resultant reduced bandgap photocatalysts have increased light absorption edge, thereby improving the H_2 production efficiency.

3.4. Composition analysis

The surface chemical composition, electronic states, and oxidation states of AFT-OA and AFT-N_2 photocatalysts were examined by XPS, in which the presence of photocatalysts (Fig. 5a), silver (Ag), titanium (Ti), carbon (C), and oxygen (O) elements were confirmed for both the catalysts. The resultant atomic weight percentages of AFT-OA and AFT-N_2 are, respectively given in the supplementary information (Table S1 and S2). From this data, AFT-OA showed lower carbon atomic weight % than AFT-N_2 catalyst due to the decomposition of FCNTs in the composite, which was subjected to calcination under the open-air conditions. The Ti $2p_{3/2}$ and Ti $2p_{1/2}$ of pristine TiO_2 binding energies are located at 458.0 eV and 463.7 eV (given in Supplementary as Fig. S1) and these peaks are ascribed to Ti^{4+} state in the TiO_2 lattice (Bharti et al., 2016). From Fig. 5b, the original binding energy values of TiO_2 were slightly shifted after the inclusion of AgNPs and carbon into TiO_2, while the new peaks are located at 458.2 and 464.1 eV. Interestingly, the peaks for AFT-N_2 catalyst also shifted compared to AFT-OA. For more detailed investigation high-resolution XPS was performed and shown in Fig. 5c. The C1s XPS analysis of AFT-OA and AFT-N_2 catalysts coordinately showed three peaks centered at 284.3, 287.8, and 288.2 eV, assigned to C═C, C–COOH, and C–O, respectively (Akhavan et al., 2011; Luo et al., 2012). However, the presence of carboxyl group indicate the formation of Ti–O–C in the composite (Sarkar and Basak, 2013). The Ag $3d_{5/2}$ and Ag $3d_{3/2}$ characteristic binding energy peaks for AFT-OA are shown at 367.5 and 373.5 eV while for AFT-N_2 at 366.6 and 372.5 eV, respectively (Fig. 5d) (Kumar et al., 2016b). These resultant binding energy peaks are slightly shifted in both the catalysts compared to the standard Ag $3d_{5/2}$ and Ag $3d_{3/2}$ peaks viz., 368.2 and 374.2 eV. This could be due to the fact that Ag exerted a strong interface interaction with FCNTs and TiO_2 (Akhavan, 2009; Zheng et al., 2007). The binding energy difference between Ag $3d_{5/2}$ and Ag $3d_{3/2}$ is ~6.0 eV, which is referred to as 3d doublet splitting energy and further represents the Ag in metallic form (Sarkar and Basak, 2013). In the case of high-resolution spectra of O1s (Fig. 5e), the peak located at 529.5 eV may be attributed to oxygen ions in the Ti lattice (Ti–O–Ti), while for AFT-N_2, the O1s peaks were slightly shifted due to lesser oxidized species formed under the N_2 atmospheric calcination (Rojas et al., 2015).

3.5. FTIR analysis

FTIR spectra of TiO_2, AT, AFT-N_2, and AFT-OA catalysts illustrated in Fig. 6 show intra-atomic vibrations effects for metal oxides such as TiO_2 are located at below 1000 cm^{-1}. However, the strong absorption peak of TiO_2 located at 730 cm^{-1} can be attributed to Ti–O and O–Ti–O vibrations of TiO_2 (Isari et al., 2020). The pristine TiO_2 and AFT-OA catalysts showed almost similar FTIR peaks, suggesting the decomposition of carbon under OA calcination. In the AT catalyst, the peaks have significantly broadened compared to TiO_2, which can be ascribed to successful incorporation of AgNPs into TiO_2 (Alsharaeh et al., 2017). A sharp peak at 1625 cm^{-1} represents H–O–H bonds vibration (Li et al., 2005; Qian et al., 2005). The limited oxygen bonds and/or oxygen

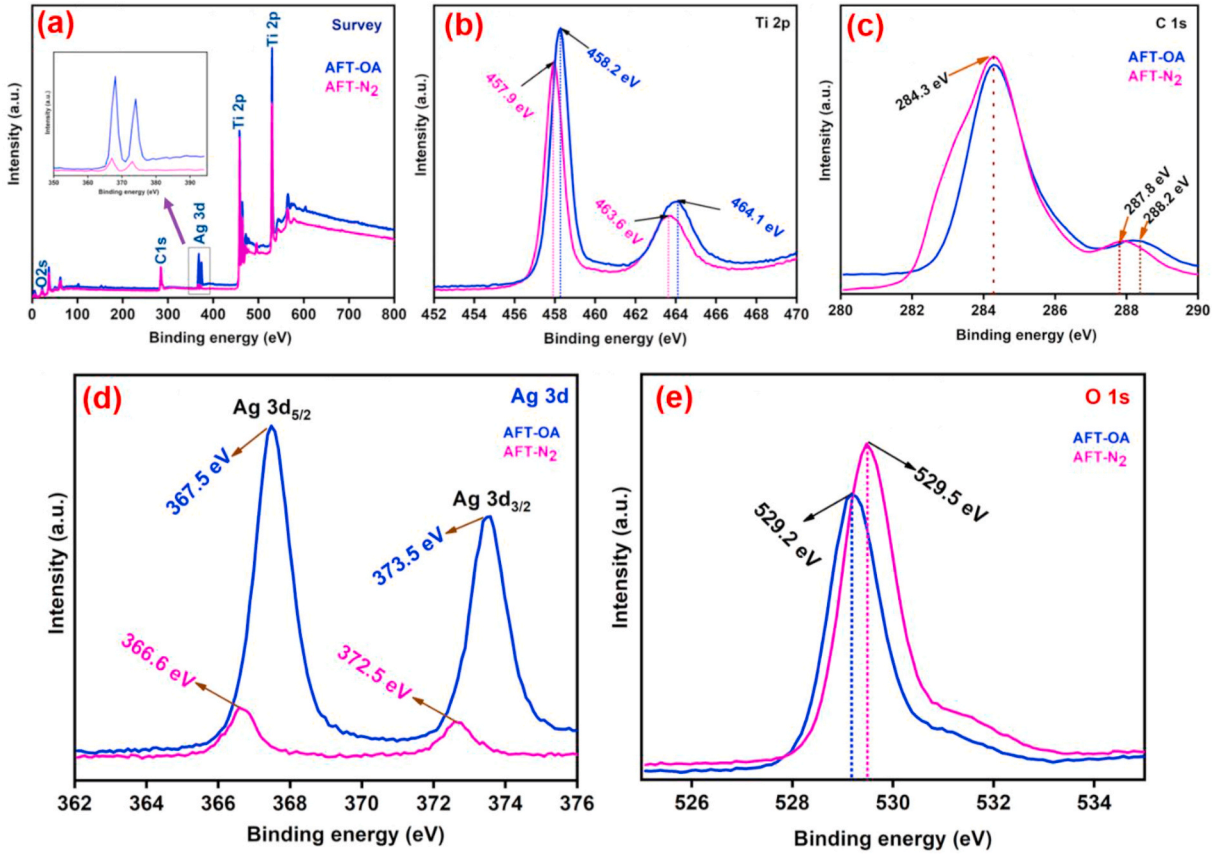

Fig. 5. XPS spectra of AFT-OA and AFT-N_2 catalysts, (a) XPS survey spectrum, the high-resolution spectrum of (b) Ti2p, (c) C1s, (d) Ag3d, and (e) O1s spectrum.

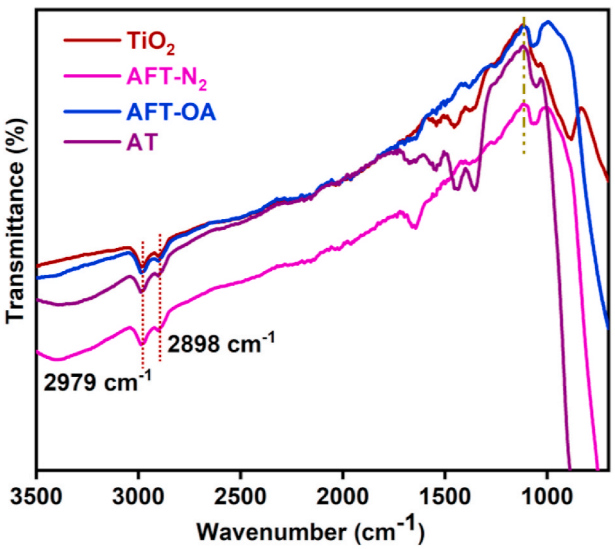

Fig. 6. FTIR spectra of TiO_2, AFT-N_2, AFT-OA, and AT catalysts.

deficiency of AFT-N_2 catalysts, resulted in the shift of FTIR peaks showing fewer peaks compared to AFT-OA and TiO_2 catalysts. The peaks at 2982 and 2898 cm^{-1} in all the catalysts represent –CH and –COH vibrations (Chuang and Chen, 2009).

FTIR studies were also performed to see spectral changes in the optimized catalyst before and after catalytic tests (Fig. S2). In the case of FTIR spectra of optimized photocatalyst after photocatalytic measurements, there were only shifting of main peaks by 10-15 cm^{-1} in comparison with FTIR spectra of pure photocatalysts before the catalytic test, indicating that shifting of peaks in the catalyst after catalytic tests are probably due to adsorption of light by main groups present in the catalysts during the photocatalytic process. Previous studies also reported that there are no changes in FTIR spectra of the catalysts even after photocatalytic experiments (Cargnello et al., 2016). They compared FTIR spectra of TiO_2 nanostructured catalysts before and after using the catalyst for H_2 production and observed that both catalysts showed similar FTIR peaks.

3.6. Hydrogen production

Synthesized photocatalysts dispersed in aquesous glycerol solution under simulated solar light irradiation and hydrogen production rate at different experimental conditions are displayed in Fig. 7(a–d). Interestingly, AFT-N_2 catalyst calcined under the N_2 atmosphere showed higher H_2 rate than the dried (AFT-D) and open-air calcined catalysts (AFT-OA). Generally, the CNTs are highly stable under thermally inert atmospheric conditions and when calcination is carried out in open air at temperatures greater than 350 °C, it will react with oxygen to form CO_2 and/or will decompose. The CNTs decompose in the open air at 400–700 °C based on their purity and morphological setup, but CNTs active temperature can be as high as 2500 °C under inert atmosphere. Therefore, calcined catalyst under inert atmosphere conditions has a strong interaction with other metals, and such a strong interface could reduce recombination rate of the charge carriers, thereby improving the H_2 production efficiency.

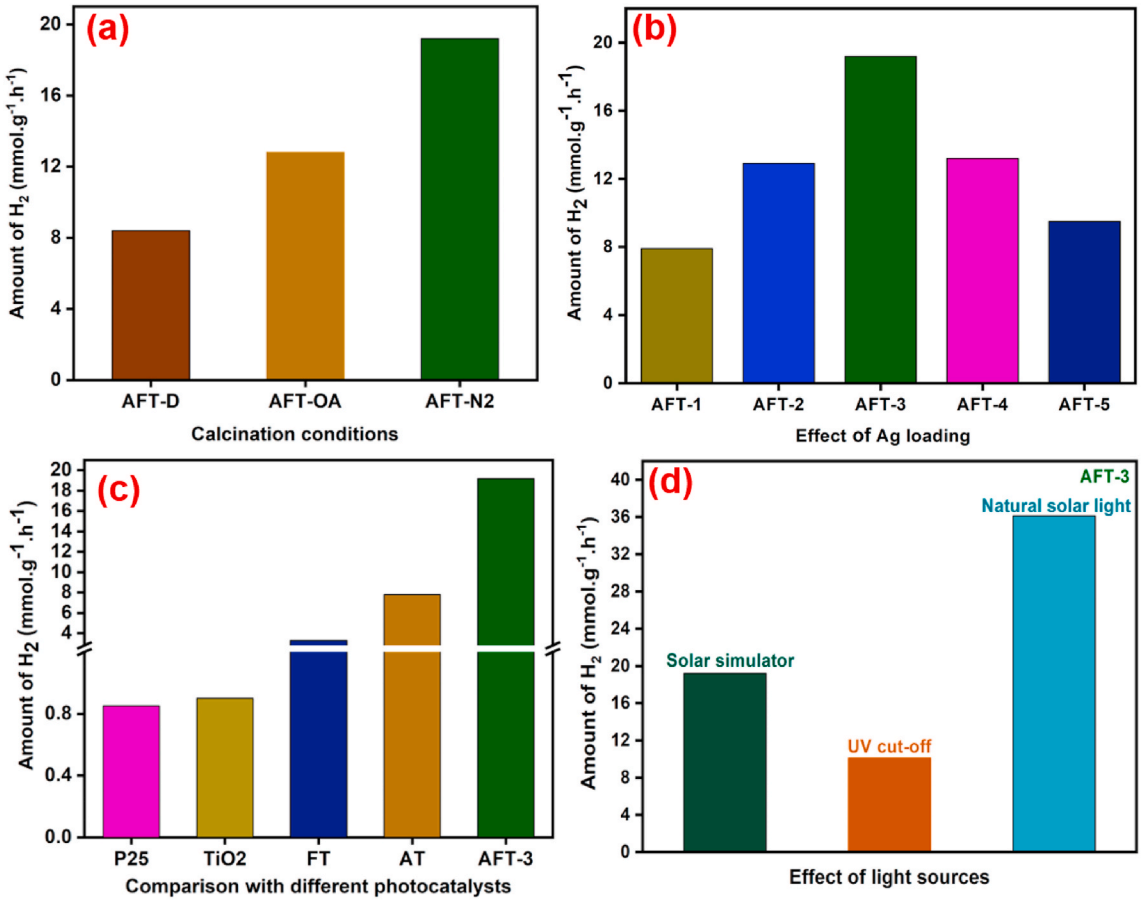

Fig. 7. Photocatalytic H_2 production assessments of Ag/FCNT-TiO_2 heterogeneous catalysts: (a) oper air and N_2 atmospheric calcination condition effect, (b) effect of silver doping concentration on FCNT-TiO_2 nanocomposite, (c) AFT-N_2 catalyst H_2 production comparison with binary (FT and AT) and pristine (TiO_2) photocatalysts and (d) Light sources effect on AFT-N_2.

The H_2 production tests were performed by varying the silver deposition contents on FCNT-TiO_2 catalyst, and these results are displayed in Fig. 7b, where AFT-3 photocatalyst showed highest H_2 production rate of 19.2 mmol g^{-1} h^{-1}. This could be due to the addition of FCNTs and AgNPs which effectively reduced the charge carrier recombination rate by acting as electron sinks and co-catalysts (Chaudhary et al., 2016a; Wang et al., 2018).

Addition of noble metal nanoparticles to FCNT-TiO_2 nanocomposite improves the photocatalytic H_2 production performance. Abdulrazzak et al., reported 20 times higher H_2 production after addition of Noble metallic particles (Pt NPs) to FCNT-TiO_2 nanocomposite. This enhanced rate is due to the co-catalyst role of noble nanoparticle usually involves in increased charge separation thereby minimizing the recombination rate of electron-hole pair (Abdulrazzak et al., 2016). Estahbanati et al., also reported the improved H_2 production rate in TiO_2@CS composite after the addition of Pt nanoparticle (Karimi Estahbanati et al., 2019). The optimized photocatalyst (AFT-3) H_2 production details are compared with the pristine TiO_2, commerical TiO_2 (P25) as well as FT and AT binary catalysts (Fig. 7c). The synthesized TiO_2 showed H_2 production rate of 0.85 mmol g^{-1} h^{-1} which is nearly same as that of commercialized P25 (0.9 mmol g^{-1} h^{-1}).

The ternary photocatalyst showed the highest H_2 production rate than the binary (FT and AT) and the pristine TiO_2 catalyst. The highest H_2 production could be due to the SPR effect of silver nanoparticles, due to the induced SPR effect (of AgNPs) showing absorption in the visible region and forming localized electrical field. Moreover, the FCNTs act as co-catalyst and electron sink, resulting in hindered recombination rate, prolonged life time as well as effectively transferring electrons to the reduction process. Also, AgNPs directly act as co-catalyst, which can trap the excited electrons from TiO_2 CB and participate in reduction reactions. Additionally, photocatalytic H_2 production activity of the optimized AFT-3 catalyst was also performed under natural solar light irradiation and simulated solar light equipped with the UV-cut off filter (Fig. 7d). Interestingly, natural solar light irradiation showed 41.1 mmol g^{-1} h^{-1} H_2 production, which is ~2.2 times greater than solar simulator irradiation, suggesting that natural solar light is a more effective to produce H_2 than the solar simulator. The use of natural solar light for H_2 production is anyway an eco-friendly and cost-effective process, and hence, there is no need for high-cost instruments. Moreover, under the UV-cut off irradiation H_2 activity can be observed and thus it is evident that, the catalysts are also active in the visible light which was further confirmed by the UV-DRS characterization. Further, photocatalytic H_2 production activity of the present work was compared with related works, the comparison is summarized in Table 2.

Recyclability of the photocatalyst was investigated on the AFT-3 catalysts for ten repeated cycles under identical conditions, where the H_2 production rate decreased after the 5^{th} cycle (Fig. 8a), possibly due to the reduced glycerol (hole scavenger) concentration in the reaction solution (Maria Magdalane et al., 2018; Reddy et al., 2017). In order to confirm whether it is due to the decrease in glycerol concentration or catalysts effect, Glycerol (5 vol.%) was added to the same reaction solution in the system after the completion of 7^{th} cycle. Interestingly, the activity was increased in the next cycles, which was almost equal to the initial cycles, suggesting the depletion of glycerol by oxidation, thereby limiting the rate of H_2 production. Further, the optimized catalyst H_2 production stability was measured continuously under long-term solar irradiation. As shown in Fig. 8b, the AFT-3 photocatalyst showed high stability upto 50 h, suggesting the potential of the catalysts for long-term practical applications. The slow H_2 production rate was observed after 50 h, indicating that after 50 h, there was no further improvement in H_2 production. This is due to sacrificial agent (glycerol) being converted into CO_2 and O_2 by the oxidation process as well as large number of products are deposited on the catalysts (Rangappa et al., 2020).

3.6.1. *Mechanism of photocatalytic H_2 production*

The band edge potentials for TiO_2 and AFT-N_2 catalysts were calculated from the following equations (Chen et al., 2015).

Valence band edge potential (E_{VB}) = X- E_e + 0.5E_g

Conduction band edge potential (E_{CB}) = E_{VB} - E_g

Here, X is electronegativity of the semiconductor, E_e is the energy of free electrons and E_g is the bandgap of the catalyst. The estimated E_{cb} and E_{vb} of TiO_2 are −0.32 eV and 2.88 eV, respectively, while for AFT-N_2 catalyst, E_{cb} and E_{vb} values are −0.39 eV and 2.55 eV, respectively. These results suggest improved E_{cb} of AFT-N_2 that might have enhanced the H_2 production efficiency. The photocatalytic H_2 generation process in AgNps doped FCNT-TiO_2 is schematically represented in Fig. 8c. The electron-hole pair generated on the TiO_2 under the irradiation of light source. The electron-hole recombination time was prolonged by the trasfer of electrons from TiO_2 to the surface of co-catalyst through heterogenous contact between Ag, FCNTs, and TiO_2. The migrated electrons effectively reduced the H^+ ions, leading to H_2 production. The FCNTs have high electrical conductivity as well as the electron storage capacity, thereby acting as electron sink, thus effectively preventing the charge carrier recombination (Kumar et al., 2018). On the other hand, glycerol acts as a hole scavenger, which reacts with the holes and forms H^+ and oxidized intermediates (Lakshmana et al., 2018).

4. Conclusions

The Ag–TiO_2, FCNT-TiO_2 binary, and AgNPs-doped FCNT-TiO_2 hybrid photocatalysts were synthesized using the one-pot chemical reduction process and their properties were analyzed by UV–visible DRS, TEM, X-RD, and Raman techniques, while their chemical composition and elemental states were analyzed by X–PS. The prepared catalysts were tested for photocatalytic H_2 production under solar simulator with glycerol aqueous solution as sacrificial reagent. The optimized catalyst (AFT-3) exhibited 19.2 mmol g^{-1} h^{-1} H_2 production, which is nearly 28.5, 7, and 5 times higher than the pristine TiO_2 nanoparticles, FCNT-TiO_2 and Ag–TiO_2 nanocomposites, respectively. Such high efficiency is due to presence of silver and FCNT as they acted as the co-catalysts, thereby reducing the overall recombination rate. Moreover, FCNTs might have acted as an electron transport channel between Ag NPs and TiO_2. Interestingly, natural solar light irradiated AFT-3 showed 41.1 mmol g^{-1} h^{-1} H_2 production rate, which is ~2.2 times higher than that of the solar simulator irradiation, suggesting that natural solar light is a more effective to produce H_2 than the solar simulator.

Table 2
The photocatalytic H_2 production results of Ag doped FCNT-TiO_2 compared with previous reports.

S. No	Photocatalyst	Synthesis method	Sacrificial agent & Light source	Hydrogen Production (μ mol g^{-1} h^{-1}	References
1	Pt/MWCNT-TiO_2	Alkaline hydrothermal & Photo-deposition	Ethanol & Solar simulator	435	Zhao et al. (2014)
2	Pt/MWCNT-TiO_2	Hydrothermal & Photo-deposition	TEOA & 250 W Xe-lamp	8092	Dai et al. (2009)
3	Pt–TiO_2/CNT	Sonochemical/hydration-dehydration	Methanol & 365 nm LED	355	Abdulrazzak et al. (2016)
4	Au/Graphene-TiO_2	Microwave assisted hydrothermal	Methanol & 420 nm LEDs	296	Wang et al. (2014)
5	Ag/TiO_2-Graphene	Hydrothermal method & microwave-assisted	Ethanol & Xenon lamp	2120	Yang et al. (2014)
6	**Ag/FCNT-TiO_2**	**Chemical reduction**	**Glycerol & 300 W Xe-lamp**	**19, 200**	**This work**

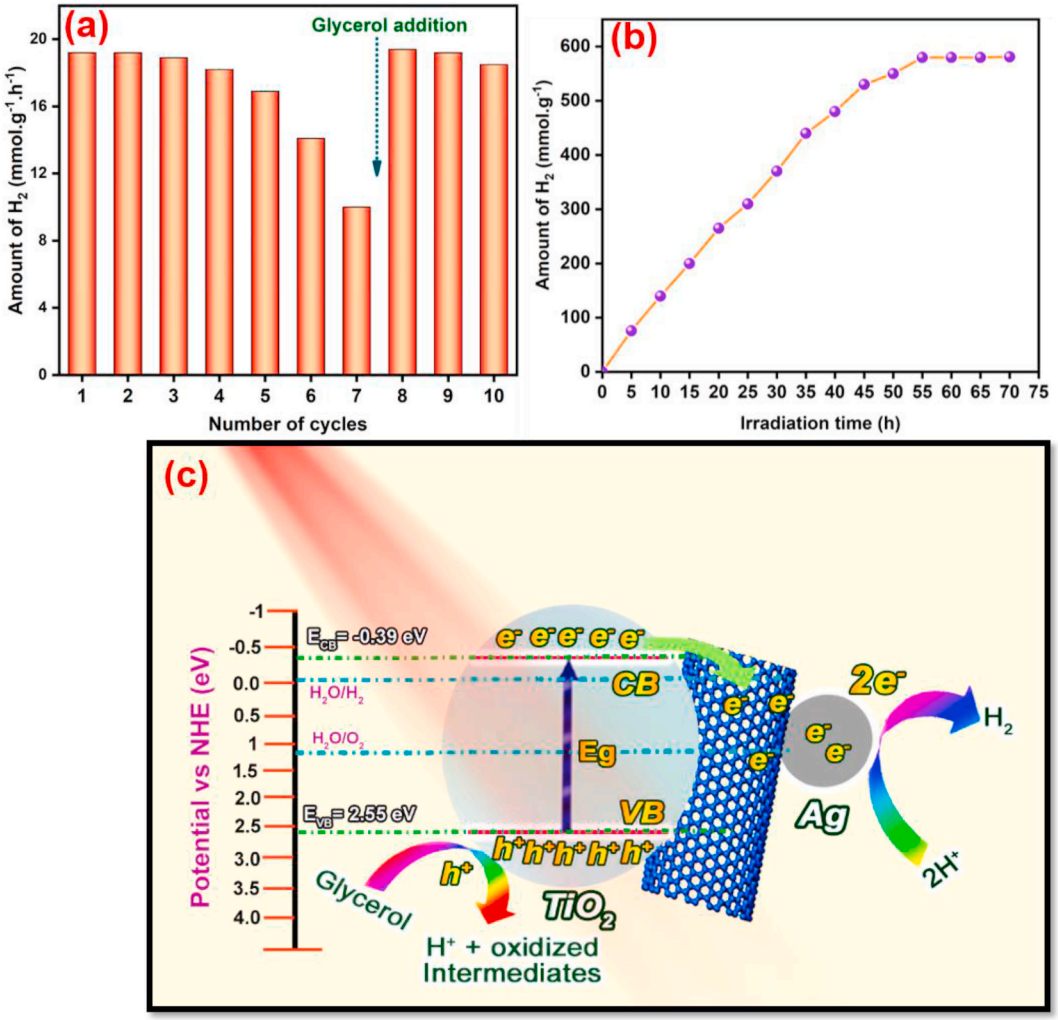

Fig. 8. (a) Recyclability tests of AFT-N_2, (b) long-term stability under continuous light irradiation, and (c) Proposed photocatalytic H_2 production mechanism with bandgap structure of AFT-N_2 under solar simulated irradiation.

As Ag nanoparticles doped FCNT-TiO_2 ternary composites have mutltifunctional properties, future scope of this work could be used in wastewater treatment applications, toxic industrial dye degradation and removal of gas pollutants applications.

Declaration of competing interest

The authors report no conflict of interest.

Acknowledgments

This work is supported by NRF-2019R1A5A8080290 of the National Research Foundation of Korea. The authors acknowledge the support from the Naval Research Board (NRB), New Delhi, India (Project No. NRB-391/MAT/17–18).

Appendix A. Supplementary data

Supplementary data to this article can be found online at https://doi.org/mmcdoino.

Credit roles

N. Ramesh Reddy: Conceptualization, Investigation, Writing – original draft, U. Bharagav: Methodology, M. V. Shankar: Writing – review & editing, Validation, P. M. Reddy: Conceptualization, Kakarla Raghava Reddy: Writing – review & editing, N. P. Shetti: Validation, Fernando Alonso-Marroquin: Writing - Reviewing & Editing, M. Mamatha Kumari: Funding acquisition, Project administration, Resources, Planning, Supervision, Tejraj M. Aminabhavi: Supervision, Reviewing & Editing, Sang Woo Joo: Funding acquisition, Project administration, Supervision.

References

Abdulrazzak, F.H., Hussein, F.H., Alkaim, A.F., Ivanova, I., Emeline, A.V., Bahnemann, D.W., 2016. Sonochemical/hydration–dehydration synthesis of Pt–TiO_2 NPs/decorated carbon nanotubes with enhanced photocatalytic hydrogen production activity. Photochem. Photobiol. Sci. 15, 1347–1357.

Akhavan, O., 2009. Lasting antibacterial activities of Ag-TiO_2/Ag/a-TiO_2 nanocomposite thin film photocatalysts under solar light irradiation. J. Colloid Interface Sci. 336, 117–124.

Akhavan, O., Azimirad, R., Safa, S., 2011. Functionalized carbon nanotubes in ZnO thin films for photoinactivation of bacteria. Mater. Chem. Phys. 130, 598–602.

Alsharaeh, E.H., Bora, T., Soliman, A., Ahmed, F., Bharath, G., Ghoniem, M.G., Abu-Salah, K.M., Dutta, J., 2017. Sol-gel-assisted microwave-derived synthesis of anatase Ag/TiO_2/Go nanohybrids toward efficient visible light phenol degradation. Catalysts 7, 1–11.

Aphairaj, D., Wirunmongkol, T., Pavasupree, S., Limsuwan, P., 2011. Effect of calcination temperatures on structures of TiO_2 powders prepared by hydrothermal method using Thai leucoxene mineral. Energy Procedia 9, 539–544.

Augustine, R., Hasan, A., 2020. Emerging applications of biocompatible phytosynthesized metal/metal oxide nanoparticles in healthcare. J. Drug Deliv. Sci. Technol. 56, 101516.

Bellamkonda, S., Thangavel, N., Hafeez, H.Y., Neppolian, B., Ranga Rao, G., 2019. Highly active and stable multi-walled carbon nanotubes-graphene-TiO_2 nanohybrid:

an efficient non-noble metal photocatalyst for water splitting. Catal. Today 321, 120–127.
Bharti, B., Kumar, S., Lee, H., Kumar, R., 2016. Formation of oxygen vacancies and Ti^{3+} state in TiO_2 thin film and enhanced optical properties by air plasma treatment. Sci. Rep. 6, 32355–32367.
Bi, Y. guang, Liu, D., 2019. Rapid synthesis of recyclable and reusable magnetic TiO_2@ Fe_3O_4 for degradation of organic pollutant. Appl. Phys. Mater. Sci. Process 125 (77).
Cargnello, M., Montini, T., Smolin, S.Y., Priebe, J.B., Delgado, J.J., 2016. Engineering titania nanostructure to tune and improve its photocatalytic activity. Proc. Natl. Acad. Sci. Unit. States Am. 1–6.
Cavalcanti, F.M., Schmal, M., Giudici, R., Brito Alves, R.M., 2019. A catalyst selection method for hydrogen production through Water-Gas Shift Reaction using artificial neural networks. J. Environ. Manag. 237, 585–594.
Chaudhary, D., Khare, N., Vankar, V.D., 2016a. Ag nanoparticles loaded TiO_2/MWCNT ternary Nanocomposite : a visible- light-driven photocatalyst with enhanced photocatalytic performance and stability. Ceram. Int. 42, 15861–15867.
Chaudhary, D., Khare, N., Vankar, V.D., 2016b. Ag nanoparticles loaded TiO_2/MWCNT ternary nanocomposite: a visible-light-driven photocatalyst with enhanced photocatalytic performance and stability. Ceram. Int. 42, 15861–15867.
Chen, Y., Fang, J., Lu, S., Xu, W., Liu, Z., Xu, X., Fang, Z., 2015. One-step hydrothermal synthesis of BiOI/Bi_2WO_6 hierarchical heterostructure with highly photocatalytic activity. J. Chem. Technol. Biotechnol. 90, 947–954.
Chuang, H.Y., Chen, D.H., 2009. Fabrication and photocatalytic activities in visible and UV light regions of Ag@TiO_2 and NiAg@TiO_2 nanoparticles. Nanotechnology 20 (105704).
Dai, K., Peng, T., Ke, D., Wei, B., 2009. Photocatalytic hydrogen generation using a nanocomposite of multi-walled carbon nanotubes and TiO_2 nanoparticles under visible light irradiation. Nanotechnology 20, 125603–125608.
Hao, C., Wang, W., Zhang, R., Zou, B., Shi, H., 2018. Enhanced photoelectrochemical water splitting with TiO_2@Ag_2O nanowire arrays via p-n heterojunction formation. Sol. Energy Mater. Sol. Cells 174, 132–139.
Isari, A.A., Hayati, F., Kakavandi, B., Rostami, M., Motevassel, M., Dehghanifard, E., 2020. N, Cu co-doped TiO_2@functionalized SWCNT photocatalyst coupled with ultrasound and visible-light: an effective sono-photocatalysis process for pharmaceutical wastewaters treatment. Chem. Eng. J. 392, 123685.
Ishaq, S., Moussa, M., Kanwal, F., Ehsan, M., Saleem, M., Van, T.N., Losic, D., 2019. Facile synthesis of ternary graphene nanocomposites with doped metal oxide and conductive polymers as electrode materials for high performance supercapacitors. Sci. Rep. 9, 1–11.
Karthik, L., Kumar, G., Kirthi, A.V., Rahuman, A.A., Bhaskara Rao, K.V., 2014. Streptomyces sp. LK3 mediated synthesis of silver nanoparticles and its biomedical application. Bioproc. Biosyst. Eng. 37, 261–267.
Kumar, D.P., Reddy, N.L., Karthik, M., Neppolian, B., Madhavan, J., Shankar, M.V., 2016a. Solar light sensitized p-Ag_2O/n-TiO_2 nanotubes heterojunction photocatalysts for enhanced hydrogen production in aqueous-glycerol solution. Sol. Energy Mater. Sol. Cells 154, 78–87.
Kumar, D.P., Reddy, N.L., Karthik, M., Neppolian, B., Madhavan, J., Shankar, M.V., 2016b. Solar light sensitized p-Ag_2O/n-TiO_2 nanotubes heterojunction photocatalysts for enhanced hydrogen production in aqueous-glycerol solution. Sol. Energy Mater. Sol. Cells 154, 78–87.
Kumar, S., Reddy, N.L., Kumar, A., Shankar, M.V., Krishnan, V., 2018. Two dimensional N-doped ZnO-graphitic carbon nitride nanosheets heterojunctions with enhanced photocatalytic hydrogen evolution. Int. J. Hydrogen Energy 43, 3988–4002.
Lakshmana Reddy, N., Krishna Reddy, G., Mahaboob Basha, K., Krishna Mounika, P., Shankar, M.V., 2016. Highly efficient hydrogen production using Bi_2O_3/TiO_2 nanostructured photocatalysts under led light irradiation. Mater. Today Proc 3, 1351–1358.
Lakshmana Reddy, N., Cheralathan, K.K., Durga Kumari, V., Neppolian, B., Muthukonda Venkatakrishnan, S., 2018. Photocatalytic reforming of bio-mass derived crude glycerol in water: a sustainable approach for improved hydrogen generation using Ni (OH)2 decorated TiO_2 nanotubes under solar light irradiation. ACS Sustain. Chem. Eng. acssuschemeng. 6 (3), 3754–3764.
Leary, R., Westwood, A., 2011. Carbonaceous nanomaterials for the enhancement of TiO_2 photocatalysis. Carbon 49, 741–772.
Li, G., Li, L., Boerio-Goates, J., Woodfield, B.F., 2005. High purity anatase TiO2 nanocrystals: near room-temperature synthesis, grain growth kinetics, and surface hydration chemistry. J. Am. Chem. Soc. 127, 8659–8666.
Li, C., Kang, N.J., Labrandero, S.D., Wan, J., González, C., Wang, D.Y., 2014. Synergistic effect of carbon nanotube and polyethersulfone on flame retardancy of carbon fiber reinforced epoxy composites. Ind. Eng. Chem. Res. 53, 1040–1047.
Liu, W.W., Aziz, A., Chai, S.P., Mohamed, A.R., Tye, C.T., 2011. The effect of carbon precursors (methane, benzene and camphor) on the quality of carbon nanotubes synthesised by the chemical vapour decomposition. Phys. E Low-Dimensional Syst. Nanostructures 43, 1535–1542.
Liu, H., Liu, S., Zhang, Z., Dong, X., Liu, T., 2016. Hydrothermal etching fabrication of TiO_2@graphene hollow structures: mutually independent exposed {001} and {101} facets nanocrystals and its synergistic photocaltalytic effects. Sci. Rep. 6, 1–12.
Lubas, M., Jasinski, J.J., Sitarz, M., Kurpaska, L., Podsiad, P., Jasinski, J., 2014. Raman spectroscopy of TiO_2 thin films formed by hybrid treatment for biomedical applications. Spectrochim. Acta Part A Mol. Biomol. Spectrosc. 133, 867–871.
Luo, Q.P., Yu, X.Y., Lei, B.X., Chen, H.Y., Kuang, D., Bin, C.Y., 2012. Reduced graphene oxide-hierarchical ZnO hollow sphere composites with enhanced photocurrent and photocatalytic activity. J. Phys. Chem. C 116, 8111–8117.
Mamathakumari, M., Praveen Kumar, D., Haridoss, P., Durgakumari, V., Shankar, M.V., 2015. Nanohybrid of titania/carbon nanotubes - nanohorns: A promising photocatalyst for enhanced hydrogen production under solar irradiation. Int. J. Hydrogen Energy 40, 1665–1674.
Mandari, K.K., Police, A.K.R., Do, J.Y., Kang, M., Byon, C., 2018. Rare earth metal Gd influenced defect sites in N doped TiO_2: defect mediated improved charge transfer for enhanced photocatalytic hydrogen production. Int. J. Hydrogen Energy 1–10.
Maria Magdalane, C., Kaviyarasu, K., Raja, A., Arularasu, M.V., Mola, G.T., Isaev, A.B., Al-Dhabi, N.A., Arasu, M.V., Jeyaraj, B., Kennedy, J., Maaza, M., 2018. Photocatalytic decomposition effect of erbium doped cerium oxide nanostructures driven by visible light irradiation: investigation of cytotoxicity, antibacterial growth inhibition using catalyst. J. Photochem. Photobiol. B Biol. 185, 275–282.
Marimuthu, S., Antonisamy, A.J., Malayandi, S., Rajendran, K., Tsai, P.C., Pugazhendhi, A., Ponnusamy, V.K., 2020. Silver nanoparticles in dye effluent treatment: a review on synthesis, treatment methods, mechanisms, photocatalytic degradation, toxic effects and mitigation of toxicity. J. Photochem. Photobiol. B Biol. 205, 111823.
Mehta, A., Mishra, A., Basu, S., Shetti, N.P., Reddy, K.R., Saleh, T.A., Aminabhavi, T.M., 2019. Band gap tuning and surface modification of carbon dots for sustainable environmental remediation and photocatalytic hydrogen production – a review. J. Environ. Manag. 250, 109486.
Mishra, A., Mehta, A., Basu, S., Shetti, N.P., Reddy, K.R., Aminabhavi, T.M., 2019. Graphitic carbon nitride (g–C_3N_4)–based metal-free photocatalysts for water splitting: a review. Carbon N. Y. 149, 693–721.
Mokhtar Mohamed, M., Osman, G., Khairou, K.S., 2015. Fabrication of Ag nanoparticles modified TiO_2/CNT heterostructures for enhanced visible light photocatalytic degradation of organic pollutants and bacteria. J. Environ. Chem. Eng. 3, 1847–1859.
Naldoni, A., D'Arienzo, M., Altomare, M., Marelli, M., Scotti, R., Morazzoni, F., Selli, E., Dal Santo, V., 2013. Pt and Au/TiO_2 photocatalysts for methanol reforming: role of metal nanoparticles in tuning charge trapping properties and photoefficiency. Appl. Catal. B Environ. 130–131, 239–248.
Praveen Kumar, D., Lakshmana Reddy, N., Mamatha Kumari, M., Srinivas, B., Durga Kumari, V., Sreedhar, B., Roddatis, V., Bondarchuk, O., Karthik, M., Neppolian, B., Shankar, M.V., 2015. Cu_2O-sensitized TiO_2 nanorods with nanocavities for highly efficient photocatalytic hydrogen production under solar irradiation. Sol. Energy Mater. Sol. Cell. 136, 157–166.
Qian, L., Jin, Z.S., Yang, S.Y., Du, Z.L., Xu, X.R., 2005. Bright visible photoluminescence from nanotube titania grown by soft chemical process. Chem. Mater. 17, 5334–5338.
Ramesh Reddy, Nallapureddy, Bhargav, U., B, C.M., M, M.K., Shankar, M.V., 2018. Multiwalled carbon nanotubes in titania based nanocomposite as trap for photoexcitons for enhanced photocatalytic hydrogen production under solar light irradiation. Mater. Res. Bull. 106, 271–275.
Rangappa, A.P., Kumar, D.P., Gopannagari, M., Reddy, D.A., Hong, Y., Kim, Y., Kim, T. K., 2020. Highly efficient hydrogen generation in water using 1D CdS nanorods integrated with 2D SnS_2 nanosheets under solar light irradiation. Appl. Surf. Sci. 508, 144803.
Rao, V.N., Reddy, N.L., Kumari, M.M., Ravi, P., Sathish, M., Neppolian, B., Shankar, M. V., 2018. Synthesis of titania wrapped cadmium sulfide nanorods for photocatalytic hydrogen generation. Mater. Res. Bull. 103, 122–132.
Rao, V.N., Reddy, N.L., Kumari, M.M., Ravi, P., Sathish, M., 2019. Photocatalytic recovery of H_2 from H_2S containing wastewater : surface and interface control of photo-excitons in Cu_2S @ TiO_2 core-shell nanostructures. Appl. Catal. B Environ. 254, 174–185.
Reddy, N.L., Kumar, S., Krishnan, V., Sathish, M., Shankar, M.V., 2017. Multifunctional Cu/Ag quantum dots on TiO_2 nanotubes as highly efficient photocatalysts for enhanced solar hydrogen evolution. J. Catal. 350, 226–239.
Rojas, Jessika, Rojas, J.V., Toro-gonzalez, M., Molina-higgins, M.C., Castano, C.E., 2015. Facile radiolytic synthesis of ruthenium nanoparticles on graphene oxide and carbon nanotubes Facile radiolytic synthesis of ruthenium nanoparticles on graphene oxide and carbon nanotubes. Mater. Sci. Eng. B 205, 28–35.
Rudzinski, W.E., Aminabhavi, T.M., 2000. A review on extraction and identification of crude oil and related products using supercritical fluid technology. Energy Fuels 14, 464–475.
Sangari, M., Umadevi, M., Mayandi, J., Pinheiro, J.P., 2015. Photocatalytic degradation and antimicrobial applications of F-doped MWCNTs/TiO_2 composites. Spectrochim. Acta Part A Mol. Biomol. Spectrosc. 139, 290–295.
Sarkar, S., Basak, D., 2013. One-step nano-engineering of dispersed Ag-ZnO nanoparticles' hybrid in reduced graphene oxide matrix and its superior photocatalytic property. CrystEngComm 15, 7606–7614.
Sreekanth, T.V.M., Jung, M.-J., Eom, I.-Y., 2016. Green synthesis of silver nanoparticles, decorated on graphene oxide nanosheets and their catalytic activity. Appl. Surf. Sci. 361, 102–106.
Su, C., Liu, L., Zhang, M., Zhang, Y., Shao, C., 2012. Fabrication of Ag/TiO_2 nanoheterostructures with visible light photocatalytic function via a solvothermal approach. CrystEngComm 14, 3989–3999.
Suh, M.J., Shen, Y., Chan, C.K., Kim, J.H., 2019. Titanium dioxide-layered double hydroxide composite material for adsorption-photocatalysis of water pollutants. Langmuir 35, 8699–8708.
Tranchard, P., Duquesne, S., Samyn, F., Estèbe, B., Bourbigot, S., 2017. Kinetic analysis of the thermal decomposition of a carbon fibre-reinforced epoxy resin laminate. J. Anal. Appl. Pyrolysis 126, 14–21.
Tuschel, D., 2019. Raman spectroscopy and polymorphism. Spectroscopy 34, 10–21.
Wang, Y., Yu, J., Xiao, W., Li, Q., 2014. Microwave-assisted hydrothermal synthesis of graphene based Au–TiO_2 photocatalysts for efficient visible-light hydrogen production. J. Mater. Chem. 2, 3847–3855.
Wang, Z., Low, Z.X., Zeng, X., Su, B., Yin, Y., Sun, C., Williams, T., Wang, H., Zhang, X., 2018. Vertically-heterostructured TiO_2-Ag-rGO ternary nanocomposite constructed

with {001} facetted TiO_2 nanosheets for enhanced Pt-free hydrogen production. Int. J. Hydrogen Energy 43, 1508–1515.
Xue, Y., Chang, Q., Hu, X., Cai, J., Yang, H., 2020. A simple strategy for selective photocatalysis degradation of organic dyes through selective adsorption enrichment by using a complex film of CdS and carboxylmethyl starch. J. Environ. Manag. 274, 111184.
Yang, Y., Liu, E., Dai, H., Kang, L., Wu, H., Fan, J., Hu, X., Liu, H., 2014. Photocatalytic activity of Ag-TiO_2-graphene ternary nanocomposites and application in hydrogen evolution by water splitting. Int. J. Hydrogen Energy 39, 7664–7671.
Zhang, B., Shi, R., Zhang, Y., Pan, C., 2013. Progress in Natural Science : materials International CNTs/TiO_2 composites and its electrochemical properties after UV light irradiation. Prog. Nat. Sci. Mater. Int. 23, 164–169.
Zhao, C., Luo, H., Chen, F., Zhang, P., Yi, L., You, K., 2014. A novel composite of TiO2 nanotubes with remarkably high efficiency for hydrogen production in solar-driven water splitting. Energy Environ. Sci. 7, 1700–1707.
Zheng, Y., Zheng, L., Zhan, Y., Lin, X., Zheng, Q., Wei, K., 2007. Ag/ZnO heterostructure nanocrystals: synthesis, characterization, and photocatalysis. Inorg. Chem. 46, 6980–6986.